*Biochimica et Biophysica Acta*, 547 (1979) 502—511


BBA 47709

# MAGNETOPHOTOSELECTION OF THE TRIPLET STATE OF REACTION CENTERS FROM *RHODOPSEUDOMONAS SPHAEROIDES* R-26

HARRY A. FRANK, JOHN BOLT, RICHARD FRIESNER and KENNETH SAUER

*Laboratory of Chemical Biodynamics, Lawrence Berkeley Laboratory, and Department of Chemistry, University of California, Berkeley, CA 94720 (U.S.A.)*

(Received December 21st, 1978)

*Key words: Magnetophotoselection; Reaction center; Bacterial photosynthesis; Triplet state (Rhodopseudomonas sphaeroides)*

## Summary

Reaction centers of the photosynthetic bacterium *Rhodopseudomonas sphaeroides* R-26, give rise to large triplet state EPR signals upon illumination at low temperature (11 K). Utilizing monochromatic polarized light to generate the EPR spectra (magnetophotoselection) we have shown that the intensities of the observed triplet signals are strongly dependent upon the wavelength and polarization direction of the excitation. These data can be used to calculate the orientations of the excited transition moments with respect to each other and with respect to the triplet state principal magnetic axes system. Our quantitative approach is to follow the procedure outlined in a previous publication (Frank, H.A., Friesner, R., Nairn, J.A., Dismukes, G.C. and Sauer, K. (1979) Biochim. Biophys. Acta 547, 484—501) where computer simulations of the observed triplet state spectra were employed.

The results presented in the present work indicate that the transition moment at 870 nm which is associated with the bacteriochlorophyll 'special pair' lies almost entirely along one of the principal magnetic axes of the triplet state. Also, the 870 nm transition moment makes an angle of approx. 60° with the 546 nm transition moment which is associated with a bacteriopheophytin. This latter result is in agreement with previous photoselection studies on the same bacterial species (Vermeglio, A., Breton, J., Paillotin, G. and Cogdell, R. (1978) Biochim. Biophys. Acta 501, 514—530).

## Introduction

Magnetophotoselection is a technique which combines the optical photoselection and electron paramagnetic resonance (EPR) experiments [1]. The

method is accomplished by exciting a randomly ordered system of molecular species with polarized light and recording its light-induced EPR spectrum with the excitation parallel and perpendicular to the static EPR field direction. Initially proposed by Kottis and Lefebvre [2] this technique has been used extensively in assigning the principal magnetic axes of the photoexcited triplet state of aromatic molecules [3—7] including chlorophylls [8] and for the study of triplet-triplet energy transfer between different aromatic compounds [6, 9—11].

Magnetophotoselection experiments have also been performed on chromatophores of the photosynthetic bacterium, *Rhodospirillum rubrum*, and a qualitative interpretation of the results was offered [12]. We have expanded on the application of this technique to photosynthetic systems. When treated quantitatively, the method can provide information about the relative orientations of the various reaction center pigments. Also, the method can serve as the link that binds optical photoselection studies on whole cells of magnetically aligned bacteria [13] to EPR experiments performed on the same systems [14]. Clearly, the determinations of the orientations that the various primary photoreactants in bacterial photosynthesis have with respect to the membranes as deduced from optical photoselection measurements [13] and from EPR experiments [14] should be consistent with the magnetophotoselection results.

Recently Vermeglio and coworkers [15] using optical photoselection techniques, have calculated the relative orientations of the transition moments of the chromophores in reaction centers of *Rhodopseudomonas sphaeroides*. They found that the absorbances at 870 nm and 546 nm which belong to the bacteriochlorophyll 'special pair' and a bacteriopheophytin, respectively, represent single transitions whose moments make an angle of approximately 60° with respect to each other.

In this paper we present a magnetophotoselection study on the same bacterial species. We have examined the light induced triplet state EPR spectra of reaction centers of *R. sphaeroides* excited by 882 nm and 550 nm light polarized parallel and perpendicular to the static EPR field direction. We have observed a dependence of the triplet lineshape on the wavelength of excitation and on the direction of polarization of the light.

Following the procedure outlined in a previous publication [14] we have computer simulated the observed triplet state spectra and calculated the orientations of the 870 nm and 546 nm transition moments with respect to the principal magnetic axes of the triplet state. Our approach is to derive distribution functions $D(\theta, \phi)$, that satisfy the equation

$$\overline{I}(|\underset{\sim}{H}|) = \int_0^{\pi} \int_0^{2\pi} I(\theta, \phi, |\underset{\sim}{H}|)\, D(\theta, \phi)\, \mathrm{d}\theta\, \mathrm{d}\phi \tag{1}$$

and calculate the triplet state EPR spectral intensity, $\overline{I}(|\underset{\sim}{H}|)$, for the broadband or polarized light excitations. $I(\theta, \phi, |\underset{\sim}{H}|)$ is the intensity of the triplet signal at field $|\underset{\sim}{H}|$, when the static EPR field is specified by the angles $\theta$ and $\phi$ (see below).

In addition to the orientation of the transition moments, zero-field splitting

parameters and relative rate constants of intersystem crossing for the triplet state are calculated.

## Materials and Methods

Reaction centers from *R. sphaeroides* strain R-26 were prepared by the method of Clayton and Wang [16]. The final ammonium sulfate precipitate was dialized against 0.01 M Tris-HCl (pH, 7.6), reprecipitated and suspended in 2% Triton X-100/0.025 M Tris-HCl (pH, 8.0). Solid sodium dithionite was added to about 10 mg/ml, and the solution was diluted with an equal volume of ethylene glycol. The final concentration of reaction centers ranged from $10^{-4}$ to $10^{-5}$ M. Careful cooling to 77 K gave clear glasses in quartz sample tubes (3 mm internal diameter). The samples could be stored in liquid nitrogen for several months.

The triplet state spectra were detected by light modulation at 33.5 Hz as described previously [14]. For excitation at 882 nm light from a 900 W xenon or a 1000 W mercury-xenon d.c. arc lamp was filtered through 5 cm of a 6% w/v aqueous solution of chromium potassium sulfate ($Cr_2(SO_4)_3 \cdot K_2SO_4 \cdot 24\ H_2O$) and a Baird-Atomic interference filter with a bandwidth of 10 nm at half-maximum transmittance. The light was focused into an open-ended flange constructed from waveguide and affixed to the front of a Varian TE microwave cavity to allow 100% transmission of light. Immediately prior to the cavity was located a Polaroid type HN-7 sheet polarizer which could be rotated through 360°. The amplitude ratios given in Table I were corrected for incomplete polarization. (At 882 nm the principal transmittance ratio is 27.) For excitation at 550 nm, light from the mercury-xenon lamp was filtered by 5 cm of a 0.2% w/v solution of *para*-nitrophenol in 2% w/v $NaHCO_3$ and focused through a Corning glass filter 1-69, an interference filter (550 nm) and a Polaroid type HN 38 sheet polarizer. For the broadband excitation, a tungsten lamp filtered by 5 cm of water was used at intensities below 25 mW/cm$^2$.

## Results

*Calculation of distribution functions*

When polarized light impinges upon a random sample of absorbing molecules, a distribution of orientations of the excited species is produced. The distribution functions describing the ensemble of triplet states excited by polarized light are derived from the probability that a transition moment, $\underset{\sim}{\mu}$, is excited by light having its electric vector, $\underset{\sim}{E}$, either parallel or perpendicular to the EPR field direction, $\underset{\sim}{H}$. Once these distribution functions are formulated, they can be used to specify the orientation of $\underset{\sim}{\mu}$ within the principal magnetic axis system of the triplet state.

We begin by writing the dot product of $\underset{\sim}{\mu}$ and $\underset{\sim}{H}$

$$\underset{\sim}{\mu} \cdot \underset{\sim}{H} = |\underset{\sim}{\mu}||\underset{\sim}{H}| \cos \beta \tag{2}$$

where $\beta$ is the angle between $\underset{\sim}{\mu}$ and $\underset{\sim}{H}$. Squaring and rearranging this equation

we get

$$\cos^2\beta = \frac{|\underset{\sim}{\mu} \cdot \underset{\sim}{H}|^2}{|\underset{\sim}{\mu}|^2 |\underset{\sim}{H}|^2} \tag{3}$$

Decomposing $\underset{\sim}{H}$ into its components along the principal magnetic axes yields

$$\underset{\sim}{H} = |\underset{\sim}{H}| \begin{vmatrix} \sin\theta \cos\phi \\ \sin\theta \sin\phi \\ \cos\theta \end{vmatrix} \tag{4}$$

where $\theta$ is the angle between $\underset{\sim}{H}$ and the $z$ magnetic axis and $\phi$ is the angle between the component of $\underset{\sim}{H}$ in the $xy$ plane and the $x$ magnetic axis. Similarly for $\underset{\sim}{\mu}$ we obtain

$$\underset{\sim}{\mu} = |\underset{\sim}{\mu}| \begin{vmatrix} \sin\theta' \cos\phi' \\ \sin\phi' \sin\phi' \\ \cos\theta' \end{vmatrix} \equiv |\underset{\sim}{\mu}| \begin{vmatrix} P_x \\ P_y \\ P_z \end{vmatrix} \tag{5}$$

where $\theta'$ and $\phi'$ are the angles locating $\underset{\sim}{\mu}$ in the magnetic axis system and are defined in the same manner as $\theta$ and $\phi$. $P_x$, $P_y$ and $P_z$ represent the projections of $\underset{\sim}{\mu}$ onto the three principal magnetic axes.

For $\underset{\sim}{E} \parallel \underset{\sim}{H}$, the probability that $\underset{\sim}{\mu}$ is excited is given by $\cos^2\beta$. The distribution function is obtained by substituting Eqns. 4 and 5 into Eqn. 3 and by considering the appropriate solid angle element. The result is

$$D_{\parallel}(\theta, \phi) = (P_x \sin\theta \cos\phi + P_y \sin\theta \sin\phi + P_z \cos\theta)^2 \sin\theta \tag{6}$$

We may now choose the best $P_x$, $P_y$ and $P_z$ values that calculate the observed triplet state spectrum when $\underset{\sim}{E} \parallel \underset{\sim}{H}$.

The distribution function for the case of $\underset{\sim}{E} \perp \underset{\sim}{H}$ is different from the parallel case in that the probability of $\underset{\sim}{\mu}$ being excited in this configuration is given by $\frac{1}{2}\sin^2\beta$. This leads to a distribution function

$$D_{\perp}(\theta, \phi) = \tfrac{1}{2}[1 - (P_x \sin\theta \cos\phi + P_y \sin\theta \sin\phi + P_z \cos\theta)^2] \sin\theta \tag{7}$$

after considering the appropriate solid angle element. We may now use Eqn. 7 in evaluating Eqn. 1 for the case where $\underset{\sim}{E} \perp \underset{\sim}{H}$.

*Simulation of the observed triplet state spectra*

Our method essentially follows that described in a previous publication [14] where computer simulation of the amplitude ratios (Table I) experimentally determined at a number of key field positions (Fig. 1) were calculated prior to simulating the entire triplet state spectra. We proceed by discussing individually the simulations of the experimental spectra taken under three different excitation conditions.

*(1) Broadband excitation.* Broadband unpolarized light excites numerous transition moments of the reaction centers. This gives rise to a randomly ordered distribution of magnetic systems with respect to the EPR field direction. This is evidenced by the fact that the broadband spectrum agrees with a 'random' spectrum generated by monochromatic polarized light: the sum of one 'parallel' spectrum plus two 'perpendicular' spectra equals a 'random' spectrum. Following Ref. 14 we set $D(\theta, \phi) = \sin\theta$ in Eqn. 1 and vary the zero-

TABLE I

EXPERIMENTAL TRIPLET STATE SIGNAL AMPLITUDE RATIOS

The amplitudes were measured at the key field positions indicated in Figs. 1, 3, and 5. The pairs of measured intensities (e.g. $X^+$ and $X^-$) were found to equal within experimental error. The amplitudes are therefore designated by a superscript ± (e.g. $X^\pm$). Numbers in parentheses indicate the range of acceptable ratios calculated from a fixed value for the uncertainty in the experimental amplitude determination.

| | $Z^\pm/X^\pm$ | $Z^\pm/Y_1{}^\pm$ | $Z^\pm/Y_2{}^\pm$ |
|---|---|---|---|
| Broadband | −2.4 (−2.7, −2.2) | −4.0 (−4.6, −3.5) | 6.2 (7.7, 5.2) |
| 882 nm | | | |
| (1) parallel | −0.28 (−0.35, −0.22) | 3.7 (13.0, 1.8) | 2.2 (4.3, 1.3) |
| (2) perpendicular | −6.0 (−8.2, −4.0) | −3.6 (−4.3, −3.1) | 9.0 (14.0, 6.5) |
| 550 nm | | | |
| (1) parallel | −2.8 (−3.6, −2.2) | −8.8 (−23.5, −5.1) | − * |
| (2) perpendicular | −1.6 (−2.4, −1.1) | −3.2 (−7.3, −1.8) | 1.6 (2.4, 1.1) |

* $Y_2{}^\pm$ amplitude was approximately zero.

field splitting parameters, $|D|$ and $|E|$, and the relative rate constants for intersystem crossing, $k_x$, $k_y$ and $k_z$, until a good fit to the experimental spectrum is obtained. The values that best fit the random triplet state spectrum of *R. sphaeroides* reaction centers are given in Table II. The calculated spectrum is shown in Fig. 2.

*(2) 882 nm excitation.* As previously mentioned, the transition moment associated with the absorption band at 870 nm represents a pure electronic transition arising from the bacteriochlorophyll 'special pair'. This absorption

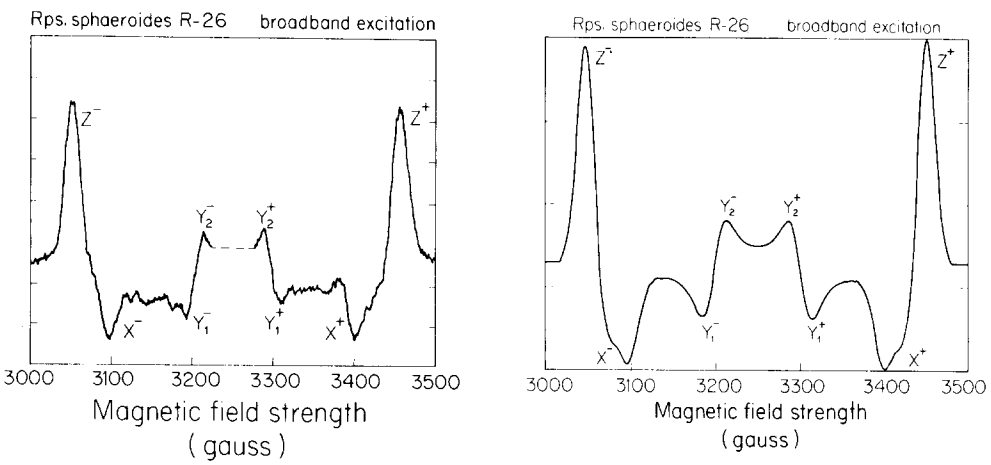


Fig. 1. Experimental triplet state spectrum of *R. sphaeroides* R-26 generated by broadband unpolarized light. Spectrum of reduced reaction centers was taken with the following conditions: sweep time, 16 min; field modulation frequency, 100 kHz; field modulation amplitude, 16 G; receiver gain, 32; temperature, 11 K; microwave power, 50 μW; microwave frequency, 9.069 GHz; light modulation frequency, 33.5 Hz; recorder time constant, 10 s; tungsten lamp excitation. The light induced free radical signal at $g = 2.0$ has been omitted.

Fig. 2. Computer simulated triplet state spectrum of *R. sphaeroides* R-26. The spectrum was calculated assuming a random distribution of triplet states with respect to the EPR field direction. The parameters used to calculate this spectrum are given in Table II.

TABLE II

ZERO-FIELD SPLITTING PARAMETERS AND RELATIVE RATE CONSTANTS FOR INTERSYSTEM CROSSING

The $|D|$ and $|E|$ zero-field splitting parameters are given in units of $cm^{-1}$. $k_x$, $k_y$ and $k_z$ refer to rate constants for depopulation of the triplet spin sublevels associated with the $X^{\pm}$, $Y^{\pm}$ and $Z^{\pm}$ triplet peaks. A comparison of the present results with published values is given.

| *R. sphaeroides* R-26 | $\|D\|$ | $\|E\|$ | $k_x : k_y : k_z$ |
|---|---|---|---|
| The present work | 0.0187 ± 0.0002 | 0.0031 ± 0.0002 | 8.3 : 7.1 : 1.0 |
| Ref. 18 | 0.0187 ± 0.0002 | 0.0031 ± 0.0001 | 1.7 : 2.0 : 1.0 |
| Ref. 19 | 0.01872 ± 0.00002 | 0.00312 ± 0.00002 | 6.4 : 5.7 : 1.0 |

is shifted to longer wavelengths at low temperatures [17]. Excitation of the molecules into their triplet states by monochromatic light at 882 nm generates an ensemble of these species whose distribution is described by Eqns. 6 and 7.

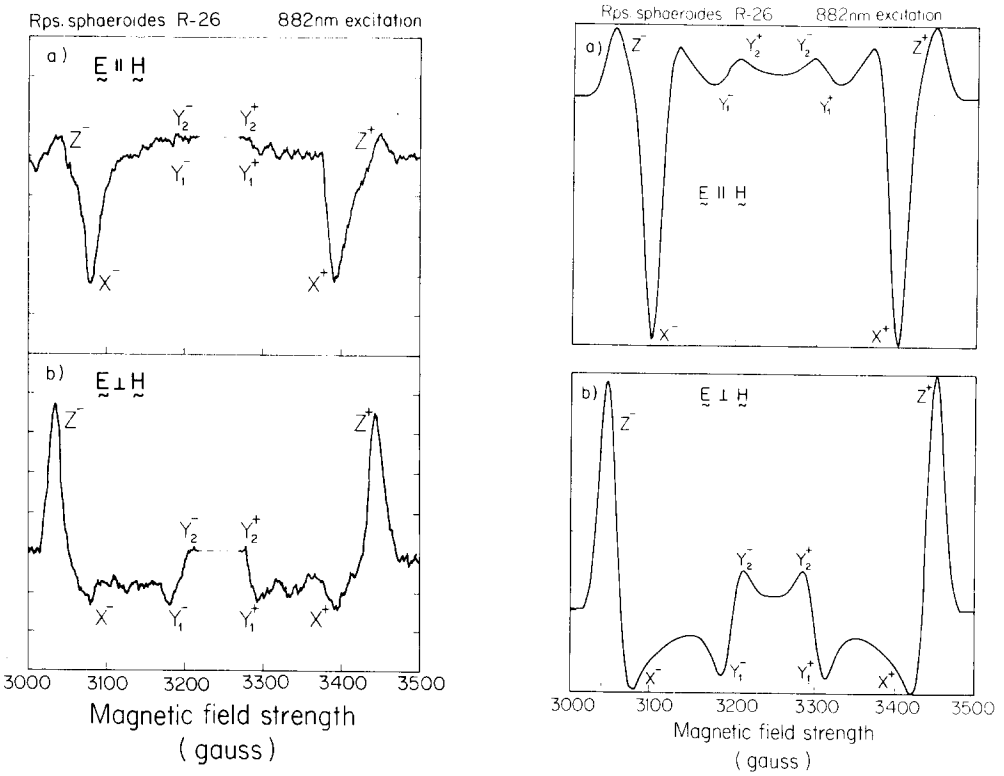


Fig. 3. Experimental triplet state spectra of *R. sphaeroides* R-26 generated by 882 nm polarized light. (a) Spectrum taken with $\underset{\sim}{E} \parallel \underset{\sim}{H}$. (b) Spectrum taken with $\underset{\sim}{E} \perp \underset{\sim}{H}$. Other conditions are as follows: sweep time, 1 h; field modulation frequency, 100 kHz; field modulation amplitude, 16 G; receiver gain, 63; temperature, 11 K; microwave power, 50 μW; microwave frequency, 9.109 GHz; light modulation frequency 33.5 Hz; recorder time constant, 30 s; xenon lamp excitation. The light-induced free radical signal at $g = 2.0$ has been omitted.

Fig. 4. Computer simulated 882 nm excited triplet state spectra of *R. sphaeroides* R-26. The spectra were calculated assuming (a) $\underset{\sim}{E} \parallel \underset{\sim}{H}$ and (b) $\underset{\sim}{E} \perp \underset{\sim}{H}$. The parameters used to calculate these spectra are given in Tables II and III. All computer simulations are normalized to the $|Z^{\pm}| + |X^{\pm}|$ peak amplitudes.

TABLE III

PROJECTION OF THE OPTICAL TRANSITION MOMENTS ONTO THE PRINCIPAL MAGNETIC AXES OF THE TRIPLET STATE

The best fit of the calculated spectra to the experimental results are given by the projections $P_x$, $P_y$ and $P_z$.

| | $P_x$ | $P_y$ | $P_z$ |
|---|---|---|---|
| 870 nm | 0.99 | 0.014 | 0.14 |
| 546 nm | 0.405 | 0.405 | 0.82 |

We assume that the $|D|$, $|E|$, $k_x$, $k_y$ and $k_z$ values are fixed by the broadband simulation (see Table II). Therefore, $P_x$, $P_y$ and $P_z$ are the parameters to be varied in calculating the amplitude ratios and simulating the experimental spectra (see Figs. 3a and 3b). We substitute Eqns. 6 and 7 into Eqn. 1 and cal-

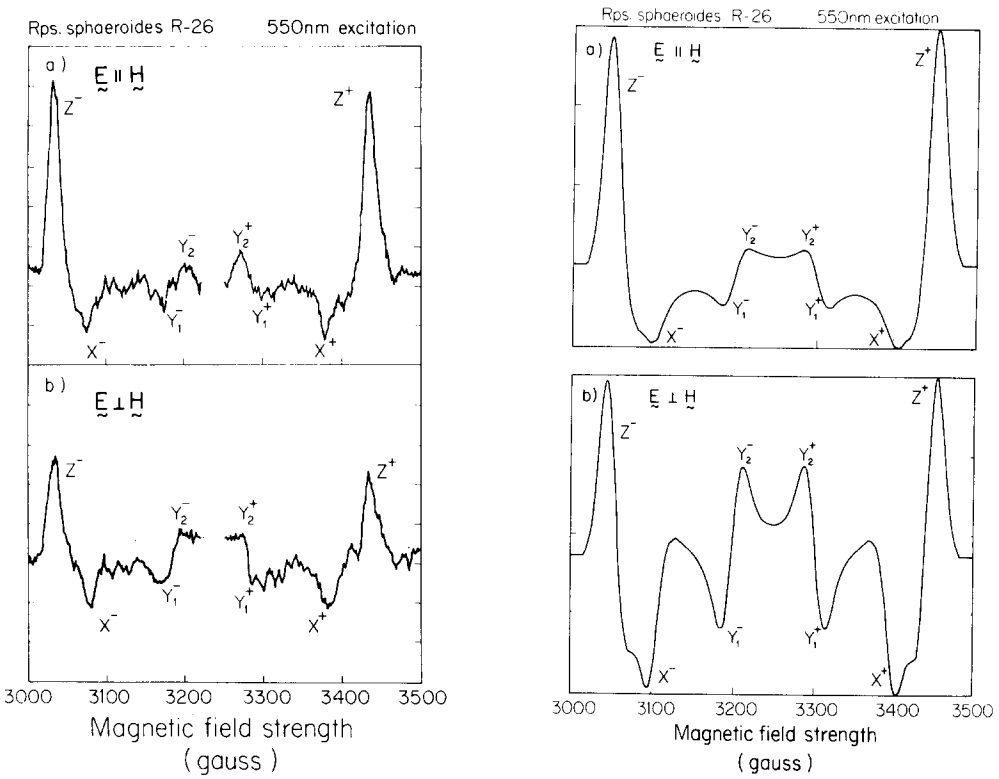


Fig. 5. Experimental triplet state spectrum of *R. sphaeroides* R-26 generated by 550 nm polarized light. (a) Spectrum taken with $\underset{\sim}{E} \parallel \underset{\sim}{H}$. (b) Spectrum taken with $\underset{\sim}{E} \perp \underset{\sim}{H}$. Other conditions are as follows: sweep time, 1 h; field modulation frequency, 100 kHz; field modulation amplitude, 16 G; receiver gain, 80; temperature, 11 K; microwave power, 50 μW; microwave frequency, 9.117 GHz; light modulation frequency 33.5 Hz; recorder time constant, 30 s; mercury-xenon lamp excitation. The light induced free radical signal at $g = 2.0$ has been omitted.

Fig. 6. Computer simulated 550 nm excited triplet state spectra of *R. sphaeroides* R-26. The spectra were calculated assuming (a) $\underset{\sim}{E} \parallel \underset{\sim}{H}$ and (b) $\underset{\sim}{E} \perp \underset{\sim}{H}$. The parameters used to calculate these spectra are given in Tables II and III.

culate the ratios for the excitation parallel and perpendicular to the static EPR field, respectively. The values for $P_x$, $P_y$ and $P_z$ that best fit the experimental results are given in Table III. The calculated spectra are shown in Figs. 4a and 4b.

*(3) 550 nm excitation.* At low temperatures absorbances associated with two different bacteriopheophytins are resolved at 530 nm and 546 nm [15,17]. Utilizing light centered at 550 nm, we excite primarily the latter species. Because the triplet state is localized on the bacteriochlorophyll 'special pair', we assume that it resides in a fixed geometric relation to the bacteriopheophytin. This allows us to use Eqns. 6 and 7 to calculate the orientation of the 546 nm transition moment with respect to the triplet magnetic axis frame. The values for $P_x$, $P_y$ and $P_z$ that best fit the amplitude ratios and the observed spectra (see Figs. 5a and 5b) are given in Table III. The computer simulated spectra for the excitation parallel and perpendicular to the static EPR field direction are shown in Figs. 6a and 6b, respectively.

## Discussion

The simulation of the broadband experimental spectrum yielded values for the $|D|$ and $|E|$ parameters that agree well with measurements from other groups [18—20] (see Table II). More interesting, however, are the values for $k_x$, $k_y$ and $k_z$ extracted by our method. Recently, there have been serious discrepancies in the numbers reported for the decay constants of *R. sphaeroides* by different groups [18,19]. Our method, which provides an independent measurement of the relative intersystem crossing rate constants, falls within the experimental error of those reported in Ref. 19.

The results that we obtained from the simulations of the triplet state spectra excited at 882 nm provide the most striking example of the accuracy in our quantitative approach. Fig. 3a shows that for $\underset{\sim}{E} \parallel \underset{\sim}{H}$ the largest component of the 870 nm transition moment lies along the $x$ principal magnetic axis *. The spectrum is dominated by the transitions associated with reaction centers where the $x$ axis is aligned along the static EPR field direction. We have determined the precise value for the projection, $P_x$, of the 870 nm transition moment onto the $x$ magnetic axis to be $0.99 \pm 0.01$. The high degree of certainty in this measurement is a consequence of the facts that the $Z^{\pm}/X^{\pm}$ ratio is very small for $\underset{\sim}{E} \parallel \underset{\sim}{H}$ and that the $Z^{\pm}/Y_1^{\pm}$ ratio is positive for $\underset{\sim}{E} \parallel \underset{\sim}{H}$ and negative for $\underset{\sim}{E} \perp \underset{\sim}{H}$. Figs. 3a and 3b show that the $Y_1^+$ and $Y_1^-$ experimental intensities are indeed positive for $\underset{\sim}{E} \parallel \underset{\sim}{H}$ and negative for $\underset{\sim}{E} \perp \underset{\sim}{H}$ while the $Z^-$ and $Z^+$ amplitudes are positive in both cases. This feature is reproduced in the simulations only when the projection of the transition moment along the $x$ principal magnetic axis is greater than 0.98. This result must arise from the summation of EPR line intensities over the ensemble distribution and is illustrative of the utility of spectral simulations in these analyses.

The observation that the $Y_1^-$ and $Y_1^+$ amplitudes are reduced significantly in absolute magnitude when the polarizer is rotated from $\underset{\sim}{E} \perp \underset{\sim}{H}$ to $\underset{\sim}{E} \parallel \underset{\sim}{H}$ indicates a small projection of the 870 nm transition moment onto the $y$ principal

* The $x$ axis defined in the present work (Figs. 1 and 7) is referred to as the $y$ axis in Ref. 8.

magnetic axis. This is borne out in the calculation showing $P_y = 0.014$. This result also argues against any significant depolarization effects arising in our system. These would substantially reduce the magnitude of the observed orientation effect. From the signal amplitudes at the $Z^-$ and $Z^+$ field positions we have calculated a projection of 0.14 for the transition moment onto the $z$ principal magnetic axis. The region of solution spanned by the two linearly independent parameters $P_x$ and $P_z$, ($P_y$ is linearly dependent because $P_x^2 + P_y^2 + P_z^2 = 1$) is shown in Table IV. No solution outside the boundaries of this rectangle fell within the experimental error.

For the 550 nm excitation, however, the rectangular region of solution is not so compact. The projections of the 546 nm transition moment onto the triplet state magnetic axes are much more uncertain owing to a less favorable signal-to-noise ratio in this determination. Nevertheless, the spectral simulations indicate a narrow range of acceptable values for the projection of the 546 nm transition moment onto the $z$ triplet state axis. Although the acceptable values for $P_x$ and $P_y$ span a fairly broad range, it is clear from the spectral simulations that the major component of the 546 nm transition moment lies along the $z$ triplet direction and has a projection of approximately 0.82 onto this axis.

Using the values of $P_x$, $P_y$ and $P_z$ listed in Table III, we can calculate the angle between the 546 nm and 870 nm transition moments. The angle is given by

$$\gamma = \arccos|\underset{\sim}{V}_1 \cdot \underset{\sim}{V}_2| \tag{8}$$

where $\underset{\sim}{V}_1 = (\pm 0.405, \pm 0.405, \pm 0.82)$ and $\underset{\sim}{V}_2 = (\pm 0.99, \pm 0.014, \pm 0.14)$ are the vectors representing the 546 nm and the 870 nm transition moments, respectively, within the principal magnetic axis system. The values for $\gamma$ calculated from Eqn. 8 are 60° (120°) and 72° (108°), which are in agreement with the 60° value determined by Vermeglio, et al. [15]. The orientations of the transition moments in the principal magnetic axis system are given in Fig. 7.

We feel that the full potential of magnetophotoselection, which is a straightforward extension of the triplet state EPR method, has not previously been fully realized in its application to photosynthetic systems. When coupled with computer simulations of the observed spectra, the technique becomes a powerful analytical tool for deciphering the orientations of the various donors and acceptors involved in the primary light reactions of photosynthesis.

Finally, any determination of the orientation of the two bacteriochlorophyll monomers with respect to each other in the 'special pair' must account for the transition moment at 870 nm lying preferentially along the $x$ principal magnetic axis of the triplet state.

TABLE IV

BOUNDARY CONDITIONS FOR THE RECTANGULAR REGION OF SOLUTION

The regions of solution are given by rectangles, the dimensions of which are determined by $P_X$ and $P_Z$ which are the projections of the transition moments onto the $x$ and $z$ principal magnetic axes, respectively.

| | | |
|---|---|---|
| 870 nm | $0.98 < P_X < 1.00$ | $0.10 < P_Z < 0.16$ |
| 546 nm | $0.33 < P_X < 0.63$ | $0.73 < P_Z < 0.85$ |

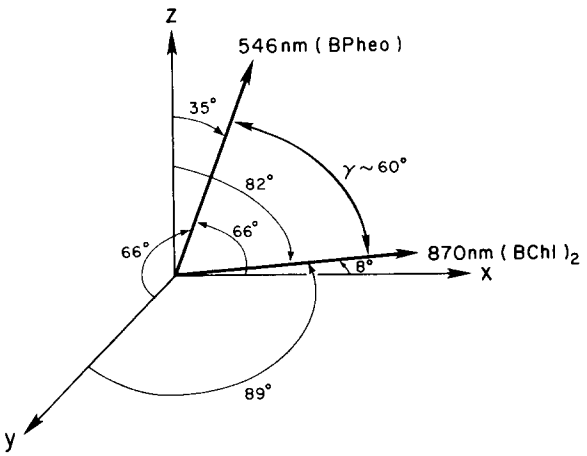


Fig. 7. The orientation of the transition moments at 546 nm and 870 nm with respect to the principal magnetic axis system ($x$, $y$, $z$) of the triplet state. The angles were calculated from the projections given in Table III using the relations $\theta_X = \arccos P_X$, etc. $\gamma$ was calculated from Eqn. 8 in the text.

## Acknowledgments

We wish to thank Dr. Jacques Breton for many stimulating discussions. This research was supported in part by the Biomedical and Environmental Research Division of the U.S. Department of Energy, by National Science Foundation Grant PCM 76-5074, and an N.I.H. National Research Service Award to H.A.F.

## References

1 McGlynn, S.P. Azumi, T. and Kinoshita, M. (1969) Molecular Spectroscopy of the Triplet State, p. 364, Prentice-Hall, Englewood Cliffs, NJ
2 Kottis, P. and Lefebvre, R. (1964) J. Chem. Phys. 41, 3660—3661
3 Lhoste, J.-M., Haug, A. and Ptak, M. (1966) J. Chem. Phys. 44, 648—654
4 Lhoste, J.-M., Haug, A. and Ptak, M. (1966) J. Chem. Phys. 44, 654—657
5 El-Sayed, M.A. and Siegel, S. (1966) J. Chem. Phys. 44, 1416—1423
6 Rabold, G.P. and Piette, L.H. (1966) Photochem. Photobiol. 5, 733—738
7 Clements, R.F. and Sharnoff, M. (1970) Chem. Phys. Lett. 7, 4—6
8 Thurnauer, M.C. and Norris, J.R. (1977) Chem. Phys. Lett. 47, 100—105
9 Siegel, S. and Goldstein, L. (1965) J. Chem. Phys. 43, 4185—4187
10 Siegel, S. and Goldstein, L. (1966) J. Chem. Phys. 44, 2780—2785
11 Siegel, S. and Goldstein, L. (1966) J. Chem. Phys. 45, 1860
12 Thurnauer, M.C. and Norris, J.R. (1976) Biochem. Biophys. Res. Commun. 73, 501—506
13 Paillotin, G., Vermeglio, A. and Breton, J. (1979) Biochim. Biophys. Acta 545, 249—264
14 Frank, H.A., Friesner, R., Nairn, J., Dismukes, G.C. and Sauer, K. (1979) Biochim. Biophys. Acta 547, 484—501
15 Vermeglio, A., Breton, J., Paillotin, G. and Cogdell, R. (1978) Biochim. Biophys. Acta 501, 514—530
16 Clayton, R.K. and Wang, R.T. (1971) Methods Enzymol. 23, 696—704
17 Clayton, R.K. and Yamamoto, T. (1976) Photochem. Photobiol. 24, 67—70
18 Clarke, R.H., Connors, R.E. and Frank, H.A. (1976) Biochem. Biophys. Res. Commun. 71, 671—675
19 Hoff, A.J. (1976) Biochim. Biophys. Acta 440, 765—771
20 Thurnauer, M.C., Katz, J.J. and Norris, J.R. (1975) Proc. Natl. Acad. Sci. U.S. 72, 3270—3274